IEEE Access
Multidisciplinary | Rapid Review | Open Access Journal

Received December 20, 2018, accepted January 31, 2019, date of publication February 18, 2019, date of current version March 20, 2019.

Digital Object Identifier 10.1109/ACCESS.2019.2899739

2D-OFDM for Optical Camera Communication: Principle and Implementation

TRANG NGUYEN, MINH DUC THIEU, AND YEONG MIN JANG, (Member, IEEE)
Department of Electronics Engineering, Kookmin University, Seoul 02707, South Korea

Corresponding author: Yeong Min Jang (yjang@kookmin.ac.kr)

This work was supported by the Institute for Information and Communications Technology Promotion (IITP) grant funded by the Korea Government (MSIT) under Grant 2017-0-00824, Development of Intelligent and Hybrid OCC-LiFi Systems for Next Generation Optical Wireless Communications.

ABSTRACT The orthogonal frequency division multiplexing (OFDM) waveform is a well-known implementation for light fidelity but quite a novel implementation for optical camera communication (OCC). This paper proposes the two-dimensional OFDM (2D-OFDM) OCC system, namely screen OCC, which implements a single screen luminaire, composed of multiple cells so that a data rate of up to 50 kb/s can be achieved with the 2D-OFDM waveform. This paper includes a mature system design based on theoretical analysis and implementation validation. The various technical details described include system architectures, theoretical analyses of the link budget, and detailed implemental guidance for the proposed Screen OFDM system. The reliability of the proposed system was verified through numerical performance measurements, as recorded that the overall BER of 10^{-5} is achievable within the communication distance of 4.5 m and the viewing angle of 30°. The overall performance of the screen OFDM is also compared with a single-carrier modulation approach, asynchronous-quick-link code within the ongoing IEEE 802.15.7m standard, to demonstrate the reliable performance of the proposing system.

INDEX TERMS Optical camera communication, OCC, OFDM, Optical OFDM, 1D-OFDM, 2D-OFDM, OFDM-OCC, screen OFDM.

I. INTRODUCTION

A. LIGHT COMMUNICATION & OUR INTERESTS

The demand for wireless communication systems has exponentially increased over the last few years, and many companies are spending the majority of their budgets hunting for novel technologies that can be used to facilitate their leadership in the potential market or meet the existing market demand. ''Out-of-the-box'' wireless technology is predicted to have massive market potential. This technology relies on the radio-interference-free spectrum, i.e., Optical Wireless Communications (OWCs). The volume of the OWC market is enormous as it has been overviewed in recent IEEE 802.15 and IEEE 802.11 tutorials [1]. The uniqueness of OWC, as well as its wide range of protocol complexity acceptance, has also been recognized [1].

The solutions of OWC are classified by the IEEE 802.15.7m Task Group (TG7m) into four categories:

(1) Existing Visible Light Communication (VLC) modes available in IEEE 802.157-2011 standard [2];
(2) Optical Camera Communication (OCC) to detect the modulated light intensity in the camera;
(3) LED Identification (LED-ID) solutions for photodiodes operating at speeds lower than that of VLC or roughly equivalent to that of OCC;
(4) High-speed Light Fidelity (LiFi) with the use of photodiodes operating at the highest speed (exceeding 1Mbps at the PHY Service-Access-Point).

The release of IEEE 802.15.7-2011 was not very successful until this moment as there were no commercial products that would profit from its specifications. On the other hand, LiFi that enables better performance and requires more complex waveforms and protocols is expected to apply to low-market volumes in specialty areas [1]. Both VLC and LiFi technologies are worthy of study. However, OCC research was considered more attractive for this study, not only because of the huge volume of its potential applications but also because of the large range of possible valuable software-based treatments, algorithms, and prototype systems that could be developed without significant concerns regarding the hardware design.

The associate editor coordinating the review of this manuscript and approving it for publication was Bora Onat.

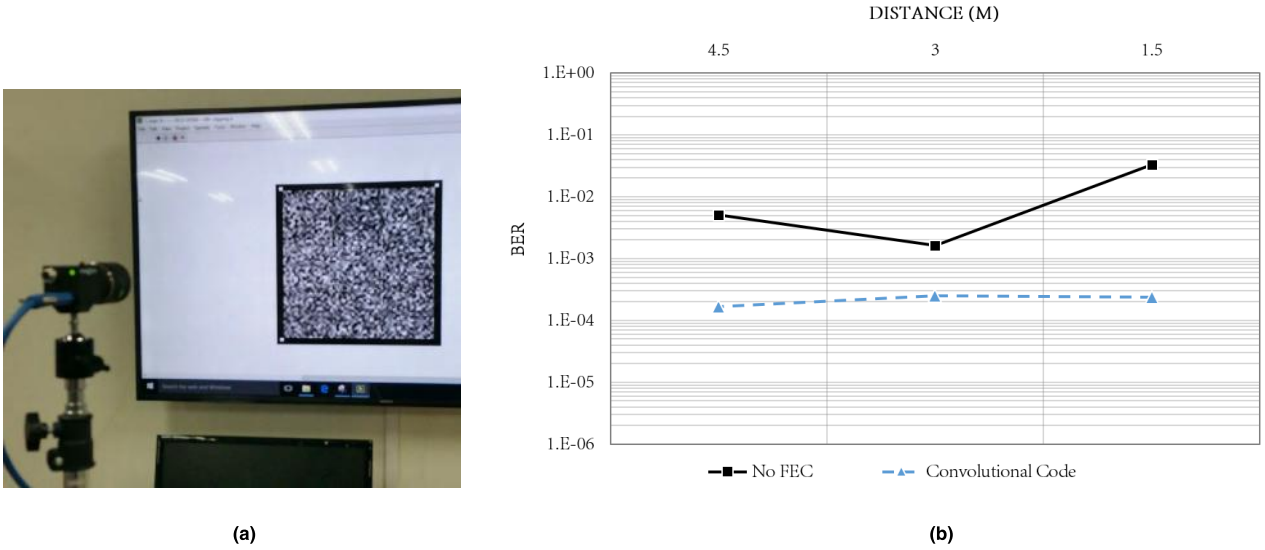

FIGURE 1. Screen OFDM system and measurement of BER performance. (a) Screen 3 × 3 MIMO-OFDM system. (b) Measured BER curves.

B. OCC CLASSIFICATION

A classification of OCC technologies in the details in [3] and [4] has disclosed that the performance of intended OCC systems is most affected by the selection of camera types. The performance barrier of OCC is caused by the communication being supplementary to the primary imaging purpose of the camera. OCC performance is primarily determined by the camera frame rate, which directly decides whether the sampling rate satisfies the Nyquist sampling requirement. The sampling manner is also determined by the shutter mechanism; the rolling shutter type camera occupies a vast segment of the camera market, while the global shutter type camera is used in specific fields to achieve higher imaging quality.

C. SCOPE OF THIS PAPER

This paper is primarily focused on Screen OCC systems. It provides a newly designed screen code supporting 2-dimensional Orthogonal Frequency Division Multiplexing (2D-OFDM).

Two-dimensional code applications, such as the statistic version of the QR code, are fading out of the market since they cannot meet the demand for higher data delivery. The dynamic version of QR could solve this issue. However, from this study and the implementation of QR codes (including an implementation of the sequential transmission of a tri-color QR code), we found that the existing code does not meet the need for sequential transmission protocol because of the huge amount of overhead per code and long delay-processing time. Indeed, the programmed sequential color QR system could deliver no more than five codes per second on a PC.

Inevitably, a new two-dimensional code design must provide good performance, comparable to QR in a specific environment, with critical features, e.g., quick detection and tracking, rotation support, and compatibility with a variety of screen infrastructures and cameras. It must also outperform QR regarding the transmission overhead and optimal frame packet. A way to support some possible modes at different data rates must be considered for some promising applications; this means that the configurations of different PHY data frame formats are critically considered. Once these challenging issues are resolved, the newly designed code can potentially replace any existing statistic-or-dynamic code in the commercial market. Asynchronous-Quick Link (A-QL) employing single-carrier modulation [4] has addressed these challenges. The advanced implementation herein, namely Screen OFDM, demonstrated even better performance.

D. THE REMAINING STRUCTURE

The rest of this paper is organized as follows.

- Section II introduces the principle of OFDM and highlights technical contributions.
- Section III recalls the fundamentals of 2D-OFDM and compares the utilized methods to those of related works.
- Section IV presents the employment details of the Screen OFDM system; the architecture along with its particular contributions are explained. The newly designed Tx and the OFDM generation procedure (including Hermitian mapping, cyclic prefix, clipping, pilots insertion, and FEC choice) are presented.
- Section V experimentally sets up the system and measures its performance against distance and perspective view to guarantee reliable performance.
- Section VI concludes the paper.

There are also additional annex sections to provide more theoretical background, clarification, and implementation guidance.

- Annex 1 analyzes the imperfections of the screen-camera channel (spatial imaging by the lens, defocus

blur, spatial sampling error, channel attenuation, and nonlinearity) and experimentally verifies the impacts of channel impairments.
- Annex 2 elaborates upon the detailed processing techniques at the receiver side required to equip critical features for Rx.

II. CONTRIBUTIONS

This first OFDM-OCC paper describes an implementation-ready screen-camera system employing a two-dimensional OFDM series. It provides the complete design of MIMO-OFDM for a screen-camera.

A. BENEFITS OF OFDM

1) GENERAL BENEFITS

The concept of OFDM has reached sufficient maturity for standardization and employment in the 1990s [5]. Recall that the OFDM system has various advantages compared to conventional single-carrier baseband modulation systems, e.g., OOK.

- OFDM, with its multicarrier modulation (MCM), splits the high bit-rate stream (in the space-time domain) into many lower bit-rate streams, i.e., each data stream is sent using an independent carrier (that is orthogonal to the other streams. This attractive feature (potentially) releases the critical need for a classic channel equalizer for a properly designed system.
- Another significant advantage of MCM is its good Inter-Symbol Interference mitigation property. The interference may come between pixels in the space-time domain or between subcarriers in the frequency-time domain for the intended screen-camera system. The channel needs to be comprehensively analyzed and modeled for clear verification, and the proper design and manipulation of OFDM need to be discussed to leverage the key resources of the system.

2) APPLYING FOR SCREEN OCC

The application of a multicarrier modulation technique to the Screen OCC system results in numerous benefits, as summarized below.

- MCM using 2D-DFT for the screen-camera system performs as well as typical 1D DFT-OFDM modulation. In the screen-camera system, the troubling of complex forms of noise (blurred image, irregular attenuation functions, and interference conditions) seems to be unmitigated in the space-time domain. The transformation of data from the space-time domain into the space-time-frequency domain brings us resolvable functions. Such the frequency-domain attenuation function H shows clearly its characteristics. Thus the dedicated allocation of orthogonal carriers can mitigate the inter-carrier interference, and the ambient light which is problematic in the single-carrier modulation can be efficiently removed in the frequency domain by ignoring the DC-component. Efficient solutions for OFDM make the system work without an expensive equalizer. These advantages make MCM (using 2D-DFT) functional as the screen-camera OCW.
- A massive MIMO Tx can be divided into smaller codes for higher link quality. In order to accomplish this approach, additional designs and the proper use of OFDM are needed. Unfortunately, even this promising approach has its drawbacks, as the bandwidth efficiency is reduced due to the required use of a cyclic prefix. There is a trade-off in selecting the size of OFDM symbols within the Tx: bigger sizes bring better bandwidth efficiency, while the smaller sizes encounter lower attenuation in the frequency domain. The sizes can be selected experimentally to compensate for the imperfect sub-bands condition.

B. TECHNICAL CONTRIBUTIONS

Throughout this study, Two-Dimensional Discrete Fourier Transform (2D-DFT) and Two-Dimensional Wavelet Transform (2D-DWT) were employed for the generation of subcarriers. 2D-DFT was mainly performed for the bi-dimensional spatial OFDM. However, a practical demonstration indicated that the DWT could be a potential alternative solution to the DFT, due to its superior and customizable sub-bands separation.

Screen OFDM is not a novel concept; however, some notable contributions of the proposed system can be highlighted as follows:

- A MIMO channel with its multiple sub-channels comprising multi-subcarriers for delivering data sequentially via the spatial-frequency domain.
- The configurable size of Tx is permitted, and its OFDM is based on the experimental verification of the channel condition in conjunction with a comprehensive analysis of channel imperfection.
- A new-and-unique design of the code (Tx) to support critical functionalities that have rarely been considered in related studies. These critical features include:
  - *360-Degree Rotation Support:* This feature is not supported by any existing Screen OFDM system and can be found solely in the QR code.
  - *Asynchronous Communication With Frame Rate Variation Support:* A sequential transmission protocol is introduced as being co-existent with a wide range of camera receivers available in the market.
  - *Correction of Perspective Distortion:* A quick correction procedure of the spatial code distortion is supported for optimal communication performance.
- Mature system architecture, detailed implemental guidance, and detailed decoding processes given based on implemental results:
  - *Rx processing* and decoding guidance.
  - *Spatial downsampling* and the correction of perspective distortion.

- *Temporal downsampling* to deal with frame rate variation.
- *Rotation correction* at Rx is done simply with matrix transpose operators.

- Moreover, the complete OFDM symbol creation and post-processing at Tx are given, as follows:
  - Spatial cyclic prefix creation and insertion.
  - Clipping processes for screen ACO-OFDM and screen DCO-OFDM.
  - Scaling and DC-bias control.
  - Effective conceptual design of 2D plots and channel equalization are introduced.
- Physical Protocol Data Unit Format (PPDU) is presented as being co-existent with 802.15 standards. As ones of the active technical contributors of IEEE 802.15.7m, our experience in the standardization is helpful for the design of new PPDU for Screen OFDM system.
- An implemental-effective FEC (one of the second generation FEC) is implemented in this system. The combining of the inner and outer FECs is natural for this system; also, it co-exists with the current and ongoing OCC standards of the IEEE Standards Association (IEEE SA).

A measurement of BER is presented in the latest section to validate BER's reliability of communication concerning the distance (up to 4.5m) and wide viewing perspective (up to 60°).

III. PRINCIPLE & RELATED WORKS

This section explains the fundamental principle of Screen OFDM and compares the proposed system to those of related studies.

A. 2D-OFDM FUNDAMENTALS

1) 2D-OFDM GENERATION

The Two-Dimensional Discrete-Time Fourier Transform (2D-DTFT) is well-known and described as a periodic transform:

$$F(u,v) = \sum_{m=-\infty}^{\infty}\sum_{n=-\infty}^{\infty} f[m,n]e^{-j2\pi(um+vn)} \tag{1}$$

Meanwhile, the 2D-DFT is known as a periodic-and-sampled transform as follows:

$$F[k,l]) = \frac{1}{MN}\sum_{m=0}^{M-1}\sum_{n=0}^{N-1} f[m,n]e^{-j2\pi\left(\frac{k}{M}m+\frac{l}{N}n\right)} \tag{2}$$

Given the mathematical principle of DTFT and DFT, the 2D-DFT can be depicted as a sampled version of the 2D-DTFT.

For the intended bi-dimensional system (i.e., screen-camera system), it is also possible to define the 2D-DFT for the image as follows:

$$F[k,l]) = \frac{1}{\sqrt{MN}}\sum_{m=0}^{M-1}\sum_{n=0}^{M-1} f[m,n]e^{-j2\pi\left(\frac{k}{M}m+\frac{l}{N}n\right)} \tag{3}$$

where $k = 0, 1, \ldots, \mathrm{M}-1$; $l = 0, 1, \ldots, \mathrm{N}-1$.

Along with that, the 2D Inverse DFT (2D-IDFT) is defined as follows:

$$f[m,n]) = \frac{1}{\sqrt{MN}}\sum_{k=0}^{M-1}\sum_{k=0}^{M-1} F[k,l]e^{j2\pi\left(\frac{k}{M}m+\frac{l}{N}n\right)} \tag{4}$$

where $\mathrm{m} = 0, 1, \ldots, \mathrm{M}-1$; $\mathrm{n} = 0, 1, \ldots, \mathrm{N}-1$.

One significant thing that cannot be ignored is, a shift-2D-DFT transform is the shifted version of a typical 2D-DFT, i.e., the shift-2D-DFT has the variables $k, l \in [-\pi, \pi]$ instead of $k, l \in [0, 2\pi]$ like the typical 2D-DFT. This issue is brought up later for the proper allocation of carrier bins.

2) 2D-OFDM ORTHOGONALITY

We can show that 2D-DFT has orthogonality, just like 1D-DFT:

$$f[m_1,n_1] = \frac{1}{\sqrt{MN}}\sum_{k=0}^{M-1}\sum_{k=0}^{N-1} F[k,l]e^{j2\pi\left(\frac{k}{M}m_1+\frac{l}{N}n_1\right)} \tag{5}$$

$$f[m_2,n_2]) = \frac{1}{\sqrt{MN}}\sum_{k=0}^{M-1}\sum_{k=0}^{N-1} F[k,l]e^{j2\pi\left(\frac{k}{M}m_2+\frac{l}{N}n_2\right)} \tag{6}$$

The orthogonality between the 2D subcarriers is shown as follows:

$$f[m_1,n_1] \perp f[m_2,n_2], \quad (m_1 \neq m_2) \vee (n_1 \neq n_2) \tag{7}$$

Undeniably, one of the significant properties of 2D-DFT is its separability. This property implies that the 2D-DFT of an image can be computed by first computing the 1D-DFT along each row of the image and then computing the 1D-DFT along each column of the intermediate result. This process can also be reversed: columns first, rows later. Since the orthogonality between the 1D-DFT subcarriers is well-known, the orthogonality inherits its property for 2D-DFT.

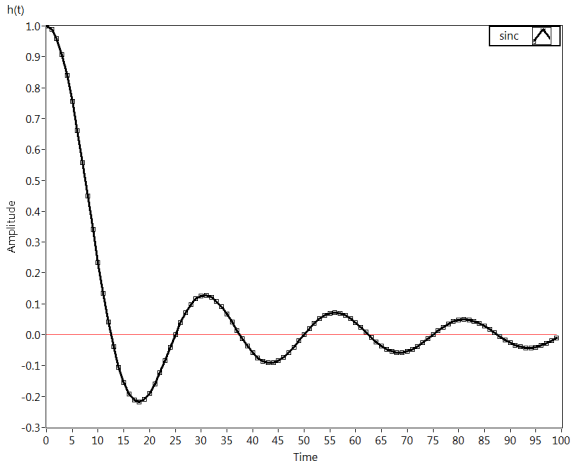

FIGURE 2. 1D-version of a sinc-function.

It is known that the sinc-function represents the impulse response h(t) of the IFFT (see FIGURE 2). Similarly, a 2D-version of the sinc-function (see FIGURE 3) represents the impulse response of the 2D-IFFT. The 2D-IDFT of

TABLE 1. Short comparison of OFDM techniques.

	ACO-OFDM	DCO-OFDM	DWT-OFDM
Modulation	QAM	QAM	QAM /PAM
MCM method	Discrete Fourier Transform	Discrete Fourier Transform	Discrete Wavelet Transform (customizable Wavelet mother and filter banks)
Complex-real conversion	Odd subcarriers Hermitian mapping	All subcarriers Hermitian mapping	Direct mapping for PAM, dual-modulator for QAM
Symbol size	2M × 2N	(2M+1) × (2N+1)	Any size
PAR and Clipping	Bias-clipping to the-top	Balanced doubled-side clipping	Lower PAPR, No clipping
CP size	Need	Need	No need
Principle Characteristic	Better power efficiency by the use of half subcarriers	Better bandwidth efficiency by the use of all subcarriers	Same bandwidth efficiency as DCO-OFDM (DCO-OFDM applies to the complex number but needs Hermitian mapping)
Implementation perspective	Lower data rate but more stable performance with noise.	Higher data rate but NULL carriers critically needed.	Half of the subbands used, PAM modulation limited. Less implemental complexity

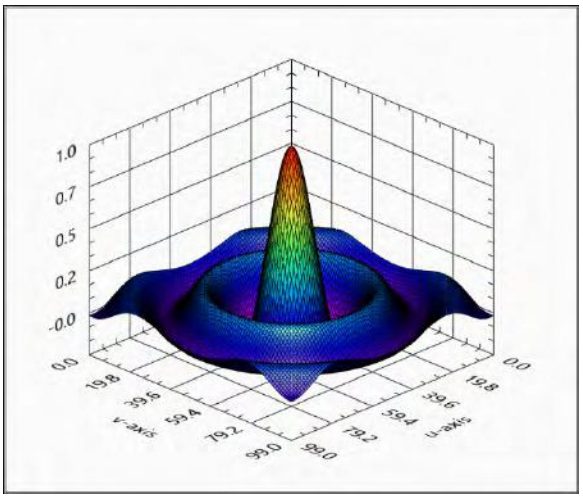

FIGURE 3. 2D-version of a sinc-function.

a 2D-rectangular wave may be quite different from the sinc-function.

B. OTHER METHODS & RELATED WORKS

1) OFDM GENERATION CHOICES

A historical implementation of OFDM was with the banks of sinusoidal. The DFT replacement has been used since the 1970s, and the maturity of DFT-OFDM was realized in the 1990s. Recently, filter-bank multicarrier has attracted researchers into OFDM.

For an OWC system, particularly for Screen OCC, the non-negative waveform required to drive light sources leads to the development of different mapping techniques prior to the IDFT. Such Asymmetrically Clipped Optical OFDM (ACO-OFDM) and DC-biased Optical OFDM (DCO-OFDM) are well-developed techniques for LiFi OFDM systems. In comparison, DWT has a variant that produces the required unipolar waveform for light sources. Table 1 briefly compares the given techniques.

Wavelet OFDM has only been standardized recently by the IEEE Standard Association (i.e., the IEEE 1901 for Power Line Network), although it provides more attractive features than FFT-OFDM (e.g., no redundancy, higher spectral separation, and reduced subchannel-interference). In a recent analysis [6], the theoretical performance of Wavelet OFDM was analyzed, and it was shown that Wavelet OFDM outperformed windowed OFDM, even with the use of less active subcarriers (sub-bands). A proper version of Wavelength OFDM in [7], theoretically showed better spectral efficiency, suppression of side-lobes, and significantly better BER. However, in practice, the typical DWT is a quadrature-mirror-filter-based, multi-scaled bandwidth separation, leading to the development of Wavelet Packet transform, i.e., a generalized version of DWT for the optical OFDM system [8]. Last but not least, an abundance of wavelet packet applications to OWC systems have been introduced in [9], demonstrating smaller PAPR and better robustness in dealing with channel imperfection.

2) RELATED WORKS

a: 2D ACO-OFDM

ACO-OFDM is popularly used for PD receiver equipped LiFi systems [10], [11]. Typical ACO-OFDM carries data through its odd subcarriers, which gives it better performance stability than DCO-OFDM. An extension of ACO-OFDM for the two-dimensional screen-camera system has been introduced in [12]. Since the NULL data was mapped onto even subcarriers, the clipping noise fell into the removable carriers at the receiving side, as demonstrated by the simulated results shown in [12].

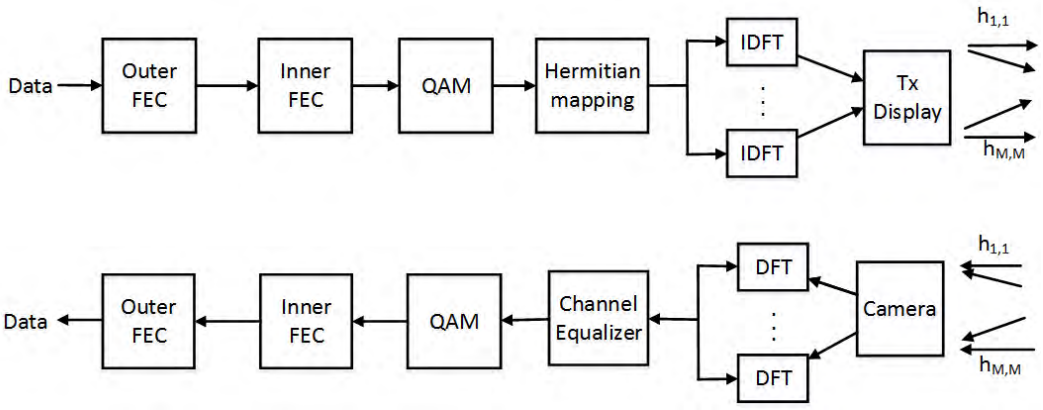

FIGURE 4. Reference architecture for the Screen-Camera DFT-OFDM system.

Given the methodology of spatial ACO-OFDM, an extensive theoretical analysis of the screen-camera channel characteristic was conducted in conjunction with its verification through experimental results and implementations.

b: 2D DCO-OFDM

An outstanding number of preferred DCO-OFDM to ACO-OFDM for VLC/LiFi systems has been investigated by research institutes and industrial companies, e.g., Fraunhofer Heinrich Hertz Institute (Germany) [13] and PureLiFi (United Kingdom) [14] because DCO-OFDM naturally provides better bandwidth efficiency when all of its subcarriers are mapped. Unlike ACO-OFDM, DCO-OFDM requires a post-processing procedure to ensure the unipolar property of the desired waveform to light source. Simple post-processing adds DC-bias to gain a non-zero waveform within the operating range of LED. Although DCO-OFDM has better bandwidth efficiency than ACO-OFDM, the allocation of NULL carriers outside the operating bandwidth is typically required.

An extension of DCO-OFDM for bi-dimensional spatial OWC systems, such as screen-cameras, has been introduced in several notable publications with significant specific features. Reference [15] introduced a concept and prototype demo for 512×512 MIMO. The measurement of the pixel amplitude response, water-pouring allocation rule for subcarriers, and theoretical analysis of channel capacity were notable. Thereafter, PixNet system [16] archived a substantially high performance, verified by experimental results. PixNet has explored the error caused by the sampling and perspective offsets; however, the mitigation of error solely depended on the perspective distortion of the existing computer vision algorithm. Eventually, the spatial DCO-OFDM (SDCO-OFDM) system [17] contributed a complementary fundamental analysis comparing SDCO-OFDM to the spatial ACO-OFDM (SACO-OFDM) under the impact of the camera lens. These three highlighted screen DCO-OFDM systems were the inspirations for this study's complete system design. Our complementary contributions, in comparison to existing works, shall be noted in each of the following implementation subsections.

c: 2D DWT-OFDM

Given the benefits of wavelets to communication systems, numerous of studies have been published in different fields of application, e.g., power line communication [6], VLC [9], optical fiber [8], and ultrawide-band vehicular communication system [18]. Advanced techniques to support DWT's outperformance of DFT have been proposed [19]. Although the IEEE SA has published its standards regarding DWT specifications in PHY [20], the applications of spatial DWT to wireless screen-camera systems are not yet as well-known as 2D-DFT. A short demo revealed the technical feasibility of 2D-DWT for OWC; however an upgraded design is needed to prove its outstanding performance.

IV. SYSTEM AND IMPLEMENTATION

A. ARCHITECTURE

A functional block diagram to implement a DFT-OFDM screen-camera system is shown in FIGURE 4.

The contributions of this proposed system are as follows:

- MIMO-OFDM screen-camera (see FIGURE 4)
  - MIMO channel with sub-channels consisting of subcarriers for reliable communication.
  - Configurable size of Tx, with OFDM symbols based on experimentally verifying the channel in conjunction with the channel analysis (see Annex 1 for the analysis of link budget).
- The new design of Tx that jointly supports critical functionalities (see FIGURE 5).
  - 360-degree rotation support.
  - Asynchronous communication with frame rate variation support.
  - Correction of perspective distortion.
- Complete system architecture and detailed implemental guidance.

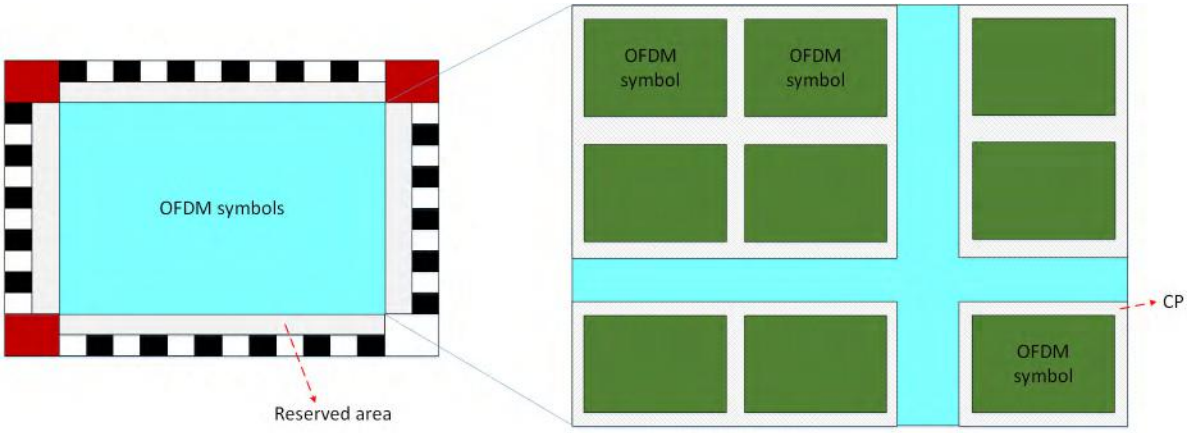

FIGURE 5. Allocation of multiple OFDM symbols to Tx.

- OFDM symbol creation and Tx post-processing (2D-cyclic prefix insertion and clipping processes).
- Scaling and DC-bias control.
- 2D pilots design and channel equalization.
- PHY frame format PPDU co-existent to 802.15 standards.
- Effective FEC.

- Comprehensive Rx processing and decoding guidance (see Annex 2).
  - Specific decoding processes are given based on implemental results, significantly including
  - Spatial downsampling and the correction of perspective distortion,
  - Temporal downsampling to deal with frame rate variation, and
  - Rotation correction.

B. TX DESIGN

The design of Tx (see TABLE 1) consists of the following features:

- The bolder area: to support the detection and extraction of the code.
- The rotation tracking corners: to determine the rotation.
- Clock cells at the surrounding of the code: to support the Rx determining the proper sampling ratio under the presence of perspective distortion.

The cyclic prefix (CP) is inserted in between the spatial OFDM symbols (see FIGURE 5) to mitigate the interference between spatial OFDM symbols. This kind of inter-spatial symbol interference always happens due to imperfect lens focusing. FIGURE 8 illustrates the allocation of the CP surrounding the OFDM symbols.

A practical example of 3×3 OFDM symbols allocated onto MIMO Tx is shown in FIGURE 6.

C. HERMITIAN MAPPING

Instead of feeding the data mapped symbol directly into the IFFT, each symbol is first arranged into a two-dimensional

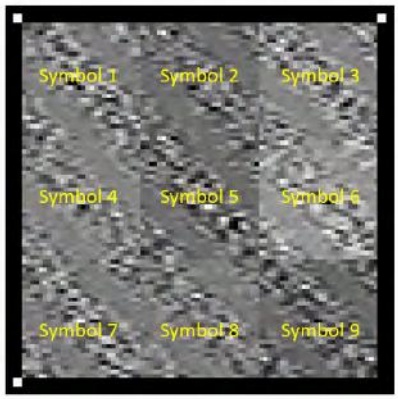

FIGURE 6. Design of 3 × 3 MIMO-OFDM Tx in the implementation.

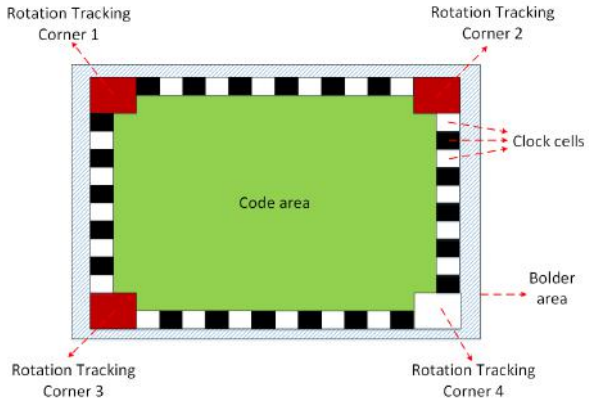

FIGURE 7. Design of Tx.

Hermitian matrix. After that, the matrix is fed into the 2D-IFFT. The special properties of the Hermitian arrangement ensure that the output of the IFFT is entirely real.

To illustrate the mapping process, denote the complex number x = (a + ib) and its conjugate $\bar{x} = (a - ib)$.

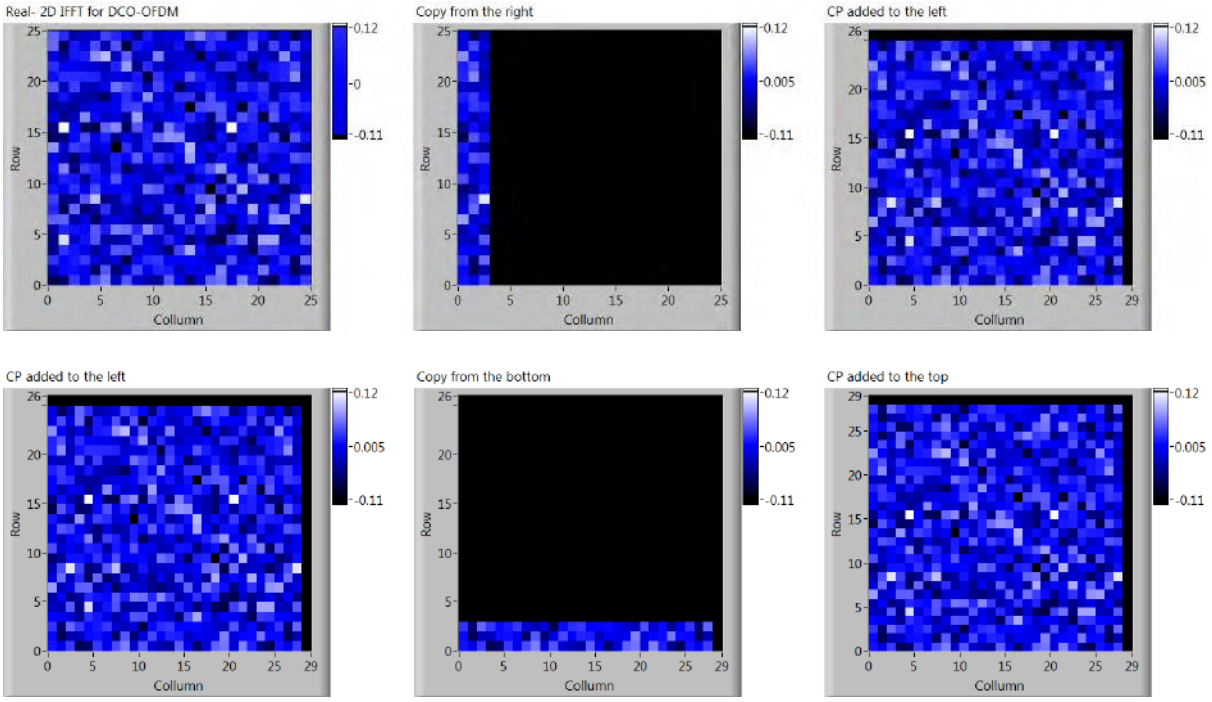

FIGURE 8. Procedure of adding the spatial Cyclic Prefix.

1) SACO-OFDM HERMITIAN MAPPING

In SACO-OFDM, to ensure the reality of the 2D-IFFT block output, all the even-index columns are set to zeros (called even subcarriers). Odd-columns carry the mapped symbols output from QAM (called odd subcarriers).

Hermitian symmetry property is arranged in the Hermitian mapping,

$$x_{i,j} = \overline{x_{M-i,\mathrm{N}+1-j}} \tag{8}$$

2) SDCO-OFDM HERMITIAN MAPPING

Assume that the size of the Hermitian matrix must be $(2k+1) \times (2k+1)$ to carry $2k \times (k+1)$ complex numbers. The 2D-IFFT shall generate $(2k+1) \times (2k+1)$ real values to be scaled and displayed on a matrix of 8-bit pixels.

The size of the real values after the 2D-IFFT operation is equal to the size of the Hermitian matrix. Thus, the size of 2D Hermitian mapping (equal to $(2k+1) \times (2k+1)$) should be considered depending on the displayed targeted resolution.

D. 2D CYCLIC PREFIX

The purpose of CP is to mitigate the interference between OFDM symbols. So, the length of CP is determined by the symbol length and time delay (un-focusing), which are variable. Typically, the CP length is about 1/8 to 1/32 of an OFDM symbol, assuming a reasonable amount of redundancy.

How CP is generated and located surrounding the OFDM symbol.

- **Step 1**: Copy the bottom rows of the OFDM symbol to form the top part of the CP.

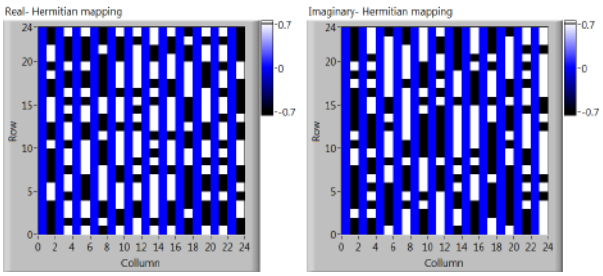

FIGURE 9. Example of Hermitian mapped symbol for ACO-OFDM.

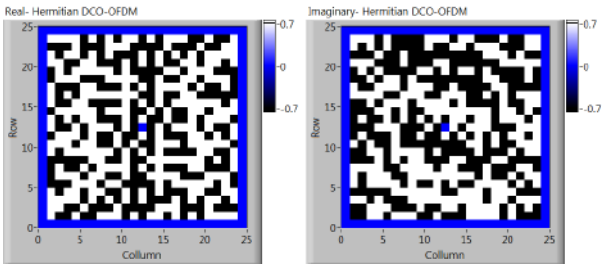

FIGURE 10. Example of Hermitian mapped symbol for DCO-OFDM.

- **Step 2**: Copy the right columns of the OFDM symbol to form the left part of the CP.
- **Step 3**: Copy the right columns of the top part of the CP to complete the CP.

E. CLIPPING

Despite the given analysis of clipping noise impact on the performance degradation (see Annex 1- Subsection 4.2),

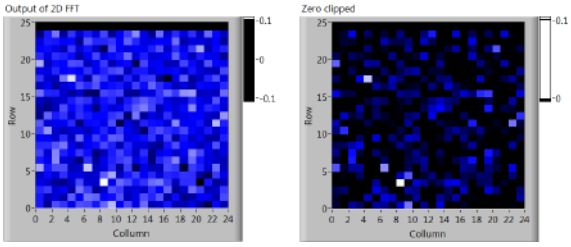

FIGURE 11. ACO-OFDM symbol output at IFFT (left) and its zero-clipped version (right).

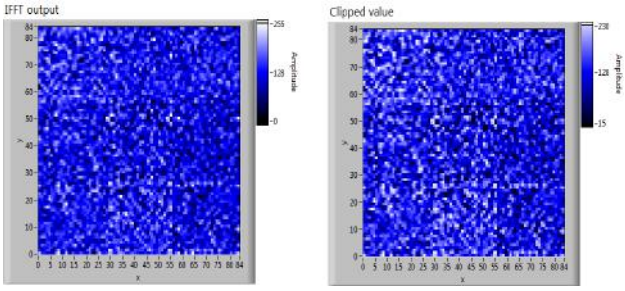

FIGURE 12. An example of clipping applied for multi-SDCO-OFDM symbols within Tx.

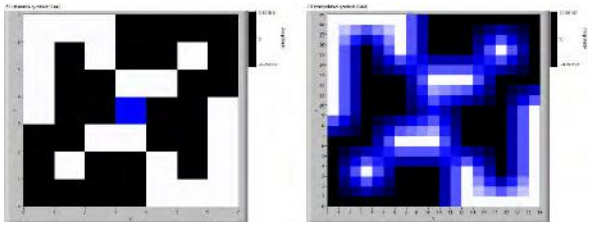

FIGURE 13. Example of bilinear interpolation using channel equalization.

the clipping is unavoidable, due to the limited range of channel intensity response. The implementation of clipping should be carefully performed for 2D ACO-OFDM and DCO-OFDM screen system as follows:

1) SACO-OFDM ZERO-CLIPPING

In 2D ACO-OFDM, the output of 2D IFFT is clipped at the zero amplitude. This zero-clipping means all negative values are set to zeros while others remain. After that, the clipping process ensures that the output can be directly modulated and transmitted by the light intensity. FIGURE 11 displays the outcome of zero-clipping at the output of ACO-OFDM modulation. ACO-OFDM zero-clipping allows the Rx canceling of all inter-carrier noise that intentionally falls in the NULL subcarriers.

Upper clipping is still needed after zero-clipping since the PAPR of the SACO-OFDM waveform is still problematic. The both-sides clipping process in the SDCO-OFDM of the following subsection covers the implementation of upper clipping in SACO-OFDM.

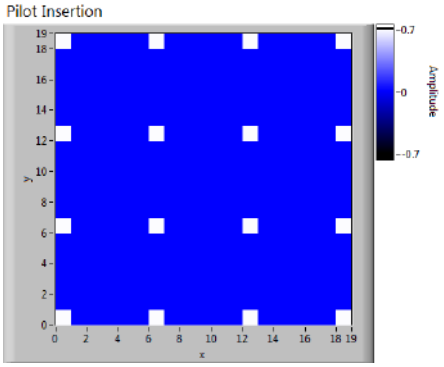

FIGURE 14. Illustration of 2D pilot positions for 2D carriers.

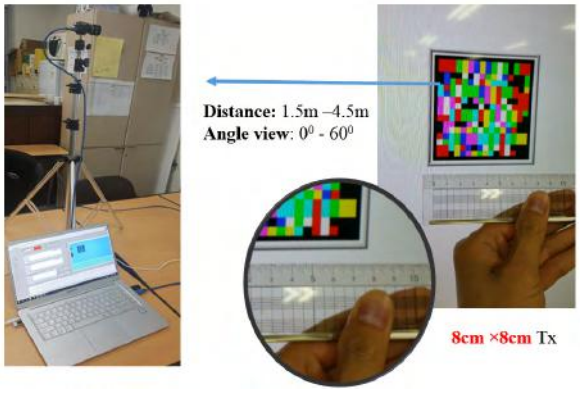

FIGURE 15. A-QL System setup for BER measurement.

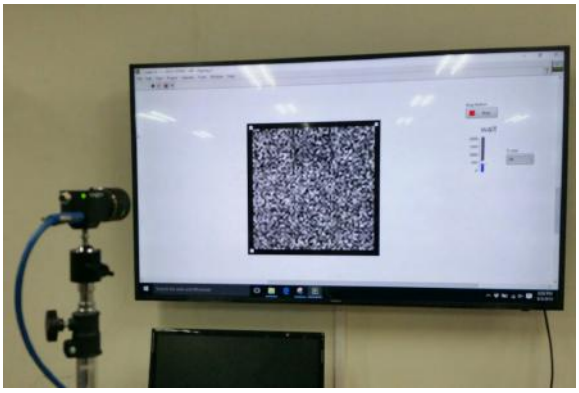

FIGURE 16. Screen-OFDM System setup for BER measurement.

2) SDCO-OFDM ZERO-CLIPPING & SCALING

Similar to the one-dimensional DCO-OFDM waveform, the modulated intensity distribution of the IFFT output is calculated for determining the lower and upper clipping thresholds (as seen in Figure 32 in Annex 1). The clipping distorts the constellation diagram, which is simulated as shown in Figure 33.

During the ending procedure, the scaling process is also applied to ensure that the modulated intensity can be

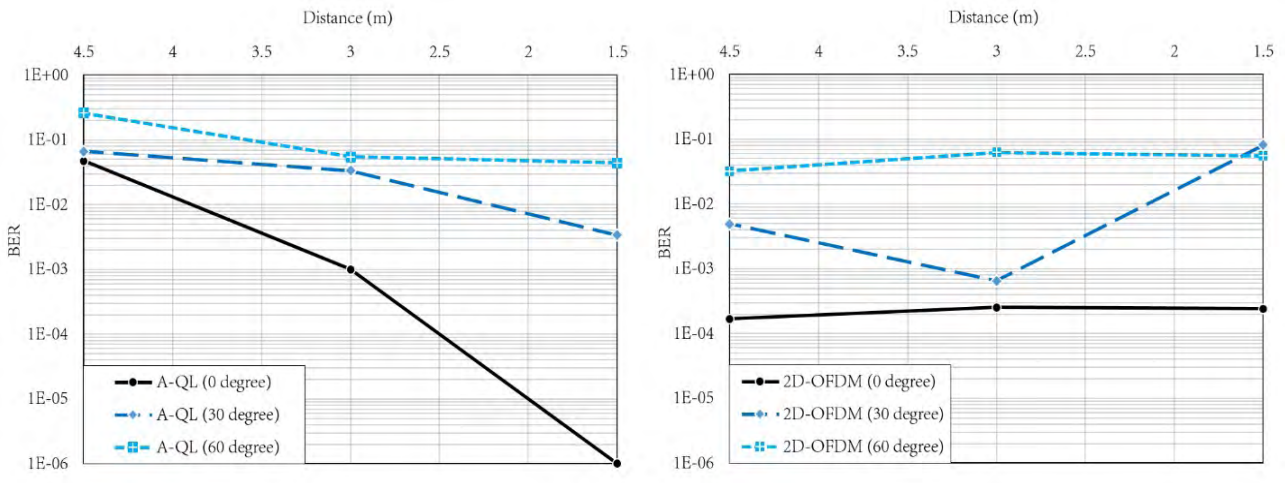

FIGURE 17. BER performance comparison between A-QL and 2D-OFDM at the Convolutional Code layer.

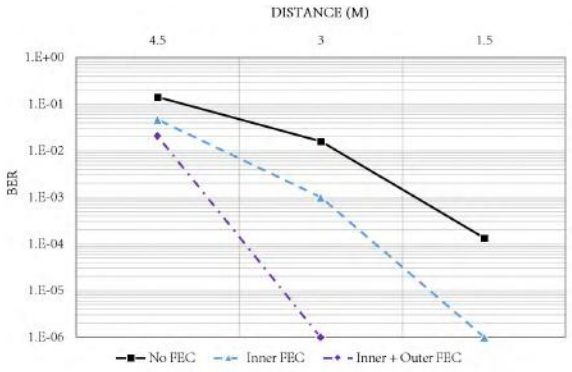

FIGURE 18. BER of A-QL system under the zero-perspective viewing angle condition.

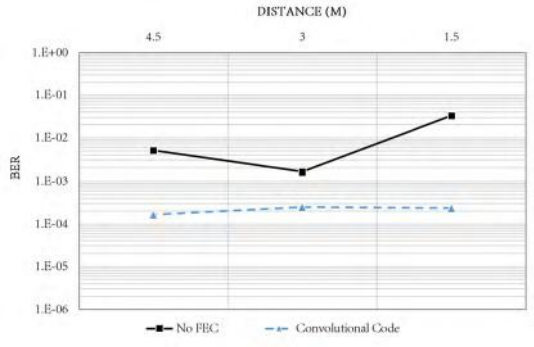

FIGURE 19. BER of Screen-OFDM system under the zero-perspective viewing angle condition.

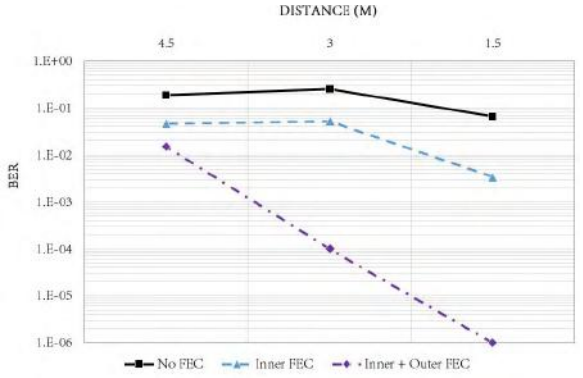

FIGURE 20. BER of A-QL system under the 30-degree perspective viewing angle condition.

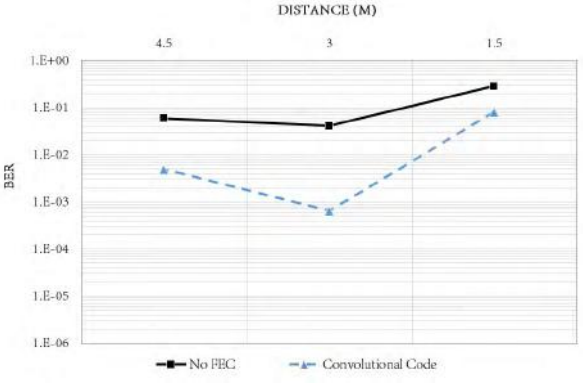

FIGURE 21. BER of Screen-OFDM system under the 30-degree perspective viewing angle condition.

displayed within the range of pixel values (e.g., 0 – 255). DC may be added to gain the desired screen brightness, if needed. FIGURE 12 shows the outcome of this process.

F. PILOTs & EQUALIZATION

1) BILINEAR INTERPOLATION

Given the 2D formation of the subcarriers, the insertion of pilots on the bi-dimensional space is reasonable. Moreover, the equalization method can be discussed in light of how the channel-impaired is a technical issue.

There is an abundance of solutions for efficient interpolation performance. However, there is always the presence of trade-off between the efficiency and complexity of any

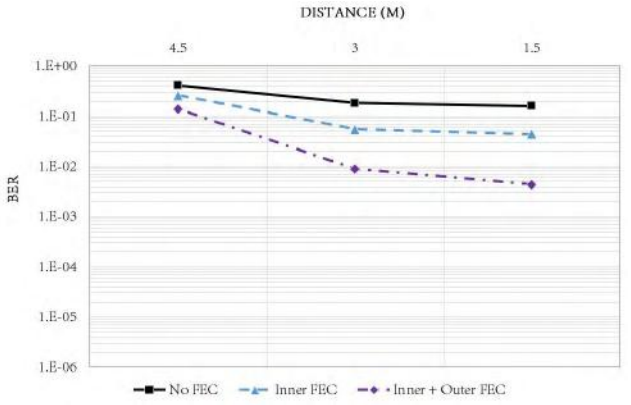

FIGURE 22. BER of A-QL system under the 60-degree perspective viewing angle condition.

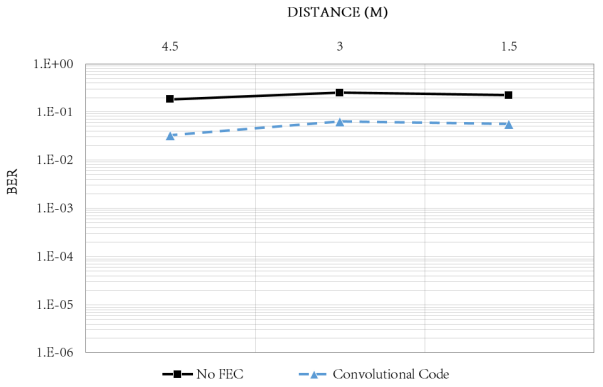

FIGURE 23. BER of Screen-OFDM system under the 60-degree perspective viewing angle condition.

method [21]. Consequently, the bilinear interpolation method is applied to equalize the 2D-channel for both simple implementation and acceptable performance. The implementation of bilinear interpolation for equalization in the 2D-frequency domain is described as follows.

The four adjacent points (four pilots, f(0, 0), f(0, 1), f(1, 0), and (1, 1)) are chosen to bilinearly interpolate the carriers in between f(x,y) as follows:

$$f(x, y) \approx f(0, 0)(1 - x)(1 - y) + f(1, 0)x(1 - y) + f(0, 1)(1 - x)y + f(1, 1)xy \quad (9)$$

This can be equivalently rewritten as a matrix operation:

$$f(x, y) \approx [1 - x \quad x] \begin{bmatrix} f(0, 0) & f(0, 1) \\ f(1, 0) & f(1, 1) \end{bmatrix} \begin{bmatrix} 1 - y \\ y \end{bmatrix} \quad (10)$$

2) PILOT SPACING

The minimal pilot density and pilot location are important for a system to endure a great deal of channel impairment. In [5], the pilot spacing applied for the 1D-OFDM symbol was analyzed; an update for the 2D-OFDM is introduced in this section.

Let $L_x \times L_y$ be the dimensions of the OFDM symbol; Δf_x, Δf_y are the spacings between subcarriers on the x-axis and y-axis.

So that $L_x \times \Delta f_x$ is the bandwidth on the x-axis and $L_y \times \Delta f_y$ is the bandwidth on the y-axis

Let τ_x, τ_y be the time delays between spatial samplings on the x-axis and y-axis, respectively. Let, T_x, T_y be the spatial sampling periods on the x-axis and y-axis respectively.

To sample the contribution of time delay, according to the sampling theorem, the maximum spacing of pilots (Δp_x and Δp_y) within the OFDM symbol must be limited to

$$\begin{cases} \Delta p_x \leq \dfrac{L_x \Delta f_x}{2\tau_x / T_x} \\ \Delta p_y \leq \dfrac{L_y \Delta f_y}{2\tau_y / T_y} \end{cases} \quad (11)$$

Perceptibly, the spacing between pilots should be close for acceptable performance of the interpolation. However, it is noted that the estimation performance is not proportional to the number of pilots. Too dense pilots may degrade the performance in case the channel is over-estimated.

Even though the channel condition varies on the distance, the size of Tx and the medium condition, practical channel attenuation, and sampling-phase shifting are measured as given in Annex 1- Figure 29 and Figure 30. We introduce the allocation of pilots as illustrated in FIGURE 14 above and it works reasonably well in the implementation.

G. FORWARD ERROR CORRECTION

For OFDM systems, different generations of FEC have been introduced. In IEEE 802.11 [22], binary convolutional coding and Low-density parity code (LDPC) are two options for OFDM PHY frame protection. In IEEE 1901-2010 [20], product encoder in conjunction with an interleaver has been introduced for FEC.

As an overall view on the development of FEC, the FEC codes are classified as three generations. Elementary BCH, RS, or CC codes are considered as the first-generation of FEC. Different concatenation schemes such as RS combined with CC, two RS combined, are commonly considered as the second generation of FEC. And the third-generation of FEC, known as codes on graphs, is with the advanced decoding technique using turbo codes and LDPC [23]. Remarkably, research on recent advanced FEC and coded modulation for the ultra-high-speed system have been discussed in details in [24].

In this system, a second generation FEC is implemented to deal with its natural PHY frame structure (CC as an inner FEC and RS as an outer FEC), in which a superframe is a time-sequence of multiple spatial frames as a combination of spatial OFDM symbols in within. The spatial frame is protected by an inner FEC, whereas an outer FEC protects the time-sequence superframe. The implementation follows the recent IEEE 802.15.7-2011 and IEEE 802.15.7-2018 (ongoing) OWC standards.

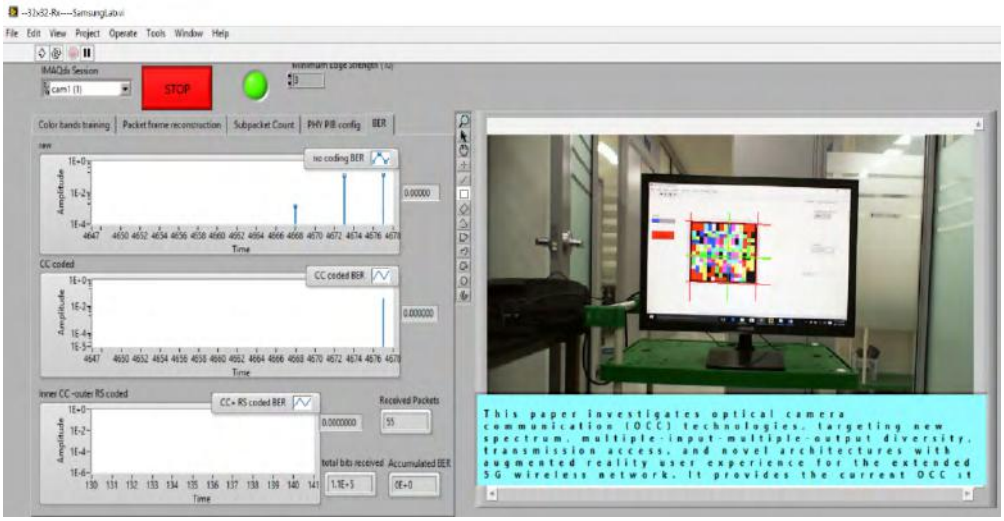

FIGURE 24. 16 × 16 A-QL Rx User Interface – Data demodulating and BER monitoring of three layers.

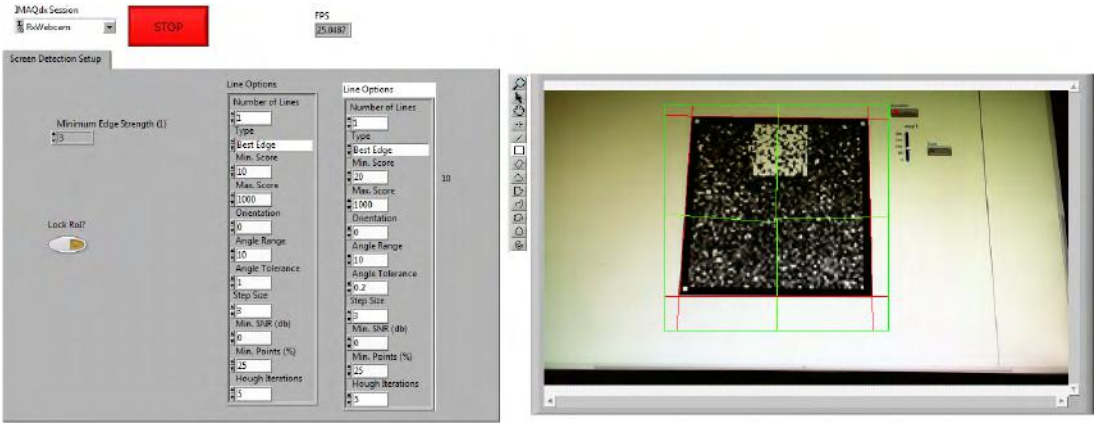

FIGURE 25. OFDM-Screen Rx Phase 1- Detecting and Extracting Tx.

V. IMPLEMENTATION RESULTS

A. SYSTEM SETUP

This section describes the performance measurement of the Screen OFDM system regarding BER under impacts of the communication distance and the perspective viewing angle. The experimental setup is captured as in FIGURE 15 and FIGURE 16.

For performance comparison, a 16 × 16 cells A-QL code (the A-QL code of the IEEE 802.15.7m ongoing standard [4]) is at the size of 8cm × 8cm, in which each Tx cell has a resolution of 5 × 5 pixel. Accordingly, for a fair BER comparison to A-QL code, the size of each element (i.e., Tx cell) of the Screen OFDM Tx must be set equal to the previous size of each cell of the A-QL system used in the measurement. Thus 5 × 5 pixels resolution (width × height) is set for the cell size of each cell element within Tx for both A-QL and Screen OFDM.

The error measured results at three layers, layer one without error correction, layer two with a Convolutional Code, and layer three (optional) with a Reed-Solomon code. The accumulated error bits is counted for many situations to practice the impacts of distance and the perspective viewing angle to BER. We checked performance at distances of 1.5m, 3m, and 4.5m; and viewing angles of 0-degree, 30-degree, and 60-degree.//

B. NUMERICAL RESULTS

Table 2 to Table 7 and FIGURE 17 to FIGURE 23 indicate the performance recorded by A-QL system and Screen OFDM system under varying conditions of distance and viewing angle. Detailed parameters used for A-QL system and Screen OFDM system are given in Table 8 and Table 9. To reveal the reliability of our implemented systems, a captured software user interfaces are illustrated in FIGURE 24 to FIGURE 26.

In comparing the practical BER curves, the performance of 2D-OFDM is more stable than A-QL versus the communication distance. Both systems have impacted by the perspective viewing angle; accordingly, the excellent correction

TABLE 2. Count of bit and error at A-QL receiver under the zero-angle view.

Distance (m)	1.5	3	4.5
Bits received	1128240	1130400	139680
Count of error (layer 1)	151	17848	19757
Count of error (layer 2)	0	0	6627
Count of error (layer 3)	0	0	2935

TABLE 3. Count of bit and error at A-QL receiver under the 30-degree view.

Distance (m)	1.5	3	4.5
Bits received	1018080	1044000	493200
Count of error (layer 1)	67121	261495	91509
Count of error (layer 2)	3448	54659	22845
Count of error (layer 3)	0	0	7379

TABLE 4. Count of bit and error at A-QL receiver under the 60-degree view.

Distance (m)	1.5	3	4.5
Bits received	442080	615600	514600
Count of error (layer 1)	70162	111953	213950
Count of error (layer 2)	19526	33881	133486
Count of error (layer 3)	1935	5475	72145

TABLE 5. Count of bit and error at Screen-OFDM Rx under the zero-perspective view.

Distance (m)	1.5	3	4.5
Bits received	1495368	1578960	1671840
Count of error (layer 1)	49317	2540	8486
Count of error (layer 2)	359	399	280

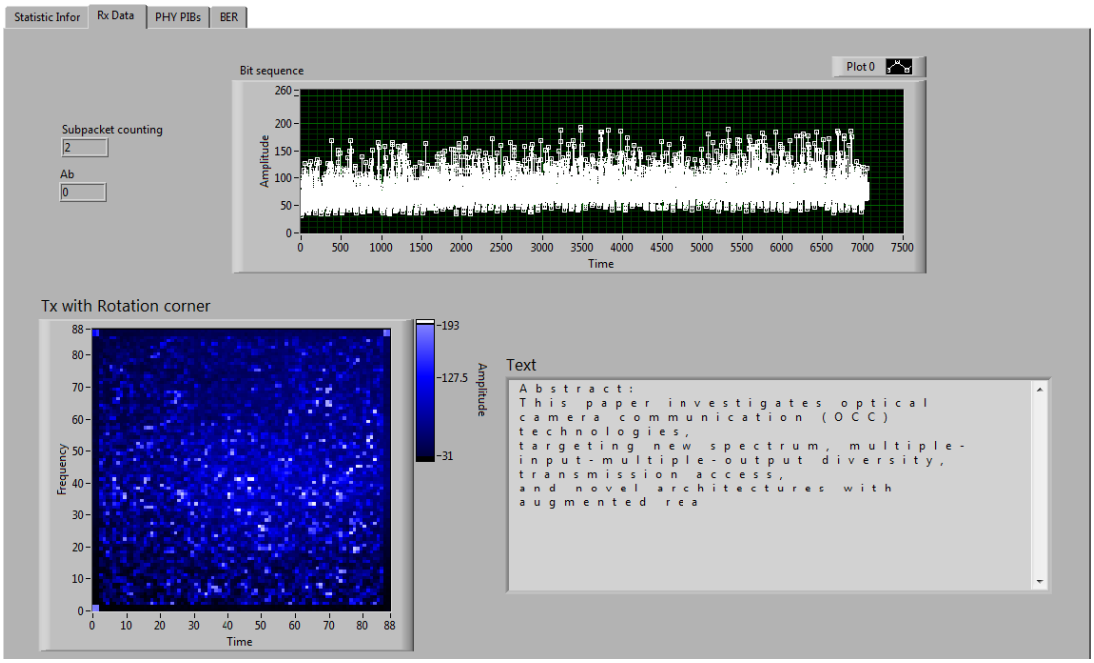

FIGURE 26. OFDM-Screen Rx Phase 2 – Demodulating data from 3 × 3 MIMO-OFDM Tx.

of perspective distortion plays an essential role for future App development to guarantee the BER against both the distance and the viewing angle.

- Screen OFDM significantly outperformed A-QL regarding BER performance for a greater communication distance and broader perspective view. Also, since the

TABLE 6. Count of bit and error at Screen-OFDM Rx under the 30-degree perspective view.

Distance (m)	1.5	3	4.5
Bits received	873072	1356048	705888
Count of error (layer 1)	253517	56267	42245
Count of error (layer 2)	71466	875	3473

TABLE 7. Count of bit and error at Screen-OFDM Rx under the 60-degree perspective view.

Distance (m)	1.5	3	4.5
Bits received	668736	566568	752328
Count of error (layer 1)	151082	144264	139067
Count of error (layer 2)	36871	35378	24219

TABLE 8. A-QL system parameters.

Number of Tx cells	16×16
Number of color bands	three
FEC	CC(1/3), RS(15,11)
Symbol clock rate	10Hz
Uncoded bit rate	7.2 kbps
Coded bit rate	1.76 kbps

TABLE 9. Screen OFDM system parameters.

Number of Tx cells	96×96
Number of symbols within Tx	3×3
Total symbol size	32×32
Occupied subcarriers	24×24
2D-DFT size	26×26
Spatial cyclic prefix	8 rows/columns surrounding
Hermitian mapping	DCO-OFDM
Modulation format	4-QAM
FEC	CC(1/3), RS(15,11)
Uncoded bit rate	51.840 kbps
Coded bit rate	12.672 kbps

allocation of subcarriers is denser at the lower bandwidth, Screen OFDM can deal with blur condition better than single-carrier A-QL.

- For BER 10-5 requirement, Screen OFDM works reliably as far as 4.5m distance with a wider perspective angle (mainly > 30 degrees) in compared to A-QL.
- If the same cell size is applied, OFDM brings better performance in compared to A-QL even with a simple channel equalizer (bilinear equalizer) used.

VI. CONCLUSION

A mature screen-camera system employing 2D-OFDM has been proposed in this first paper. The results of the theoretical analysis and implementation have been addressed in detail. Numerical results demonstrated that the implementation of the Screen OFDM system was more reliable compared to the implementation of the A-QL code even though Screen OFDM carries over ten times more data than A-QL, under the sample testing conditions.

ANNEX 1
SCREEN OFDM LINK BUDGET

A. SPATIAL IMAGING WITH LENS

1) "COSINE-FOURTH" LAW

Assume that the camera is focused, and the image of Tx is on the sensor plane. The OCC using MIMO pixels involves the inequivalent attenuation between the brightness of different cells on the Tx traveling through the optical lens to the image plane. Let Θ be the angle between the straight-entrance of the lens and the line connecting a cell to its image. The derivation of the cosine-fourth law is available in [25] and can be summarized as follows

$$\frac{E_\Theta}{E_0} = \cos^4 \Theta \tag{12}$$

where E_0, E_Θ are the illuminances received on the image plane at a point on-axis (straight to the lens entrance) and point off-axis (angled Θ to the on-axis), respectively.

As depicted in the previous equation, the illuminance on the image plane falls off as the fourth power of the cosine of the off-axis angle, where that angle is measured in "object space" from the center of the pupil entrance. This also means that the outer part of the image may get higher attenuation than the cell at the center. In fact, it is unknown which point is focused, and the focused point may also shift.

Consequently, the received pixel intensity can be calculated as

$$s'_{m,n} = \cos^4 \theta_{m,n} s_{m,n} + n_{m,n} \tag{13}$$

where $s_{m,n}$ is the signal intensity when the "Cosine-Fourth" law is not applied, and $s'_{m,n}$ is the effective intensity when the

"Cosine-Fourth" law is applied. $n_{m,n}$ is the additive noise in the space-time domain.

2) IMPACT OF THE "COSINE-FOURTH" LAW

Applying the 2D-DFT, the carriers are estimated to be

$$Y_{p,q} = \frac{1}{\sqrt{L_x L_y}} \sum_{m=0}^{L_x-1} \sum_{n=0}^{L_y-1} s_{m,n} \cos^4 \theta_{m,n} \times \exp\left(-2\pi j\left(\frac{mp}{L_x} + \frac{nq}{L_y}\right)\right) + Z_{p,q} \quad (14)$$

Carrier (p′, q′), has a relationship in the frequency domain:

$$Y_{p',q'} = \frac{1}{\sqrt{L_x L_y}} \left[S_{p',q'} \left(\sum_{m=0}^{L_x-1} \sum_{n=0}^{L_y-1} \cos^4 \theta_{m,n} \right) + \sum_{m=0}^{L_x-1} \sum_{n=0}^{L_y-1} S_{p,q} \sum_{m=0}^{L_x-1} \sum_{n=0}^{L_y-1} \cos^4 \theta_{m,n} \exp\left(2\pi j\left(\frac{m(p-p')}{L_x} + \frac{n(q-q')}{L_y}\right)\right) \right] + Z_{p',q'} \quad (15)$$

This equation has been investigated in detail in [17]; it can be shortened as follows:

$$Y_{p',q'} = S_{p',q'} H_{p',q'} + I_{p',q'} + Z_{p',q'} \quad (16)$$

where $H_{p',q'}$ is the attenuation function, and $I_{p',q'}$ is the inter-carrier interference function.

The attenuation function H is expressed as

$$H_{p',q'} = \frac{1}{\sqrt{L_x L_y}} \left(\sum_{m=0}^{L_x-1} \sum_{n=0}^{L_y-1} \cos^4 \theta_{m,n} \right) \quad (17)$$

And the inter-carrier interference I is expressed as

$$I_{p',q'} = \sum_{m=0}^{L_x-1} \sum_{n=0}^{L_y-1} S_{p,q} \sum_{m=0}^{L_x-1} \sum_{n=0}^{L_y-1} \cos^4 \theta_{m,n} \times \exp\left(2\pi j\left(\frac{m(p-p')}{L_x} + \frac{n(q-q')}{L_y}\right)\right) \quad (18)$$

where $(p - p')$ and $(q - q')$ are the spacings between the two carriers, and thus the function I represents the inter-carrier interference function of the carrier (p,q) to carrier (p′, q′).

In summary, the "Cosine-Fourth" law introduces unequal illumination to the pixels through the camera lens; as a consequence, it degrades the performance of the 2D-OFDM system by introducing the attenuation and interference between carriers in the frequency domain.

To conclude this analytical subsection, several contributions are summarized as follows. The origin and impact of a spatial imaging system have been formulated. Accordingly, the need for a 2D pilot insertion and channel equalizer has been clarified. Thus, 2D-pilots will be present in the implementation. The design and implementation of the pilot allocation are elaborated upon in the next section.

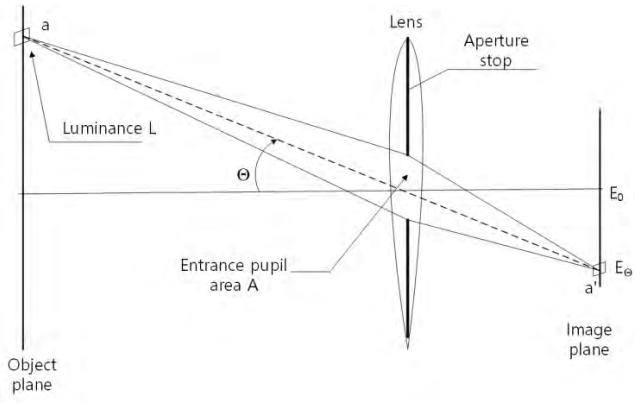

FIGURE 27. Light falloff problem in imaging, also known as natural vignetting (redrawn from [25]).

FIGURE 28. Example of a blurry image captured by the camera.

B. DEFOCUS BLUR

1) BLUR PHENOMENON

The blur effect can be simply modeled as a convolution operator:

$$s'_{m,n} = s_{m,n} \otimes h_{m,n} + n_{m,n} \quad (19)$$

where $\otimes$ represents a 2D-linear convolution; $s_{m,n}$ is the (signal) intensity without blur; $s'_{m,n}$ is the received intensity with, and $n_{m,n}$ is the additive noise.

2) BLUR IMPACT

A significant property of the DFT is that the convolution in the time domain is equivalent to the multiplication in the frequency domain, namely

$$s_{m,n} \otimes h_{m,n} \Leftrightarrow S_{p,q} H^{\otimes}_{p,q} \quad (20)$$

where $H^{\otimes}_{p,q}$ is the frequency response of the convolution h.

Thus, the output of 2D-DFT at the Rx will have a simple form as follows:

$$Y_{p,q} = S_{p,q} H^{\otimes}_{p,q} + Z_{p,q} \quad (21)$$

Observe that the blur effect contributes to the attenuation of the carriers in the frequency domain. The typical blur effect is equivalent to low-pass filtering, so that higher frequency may experience higher attenuation. The attenuation factor depends on how blurry the received image is. The attenuation can be

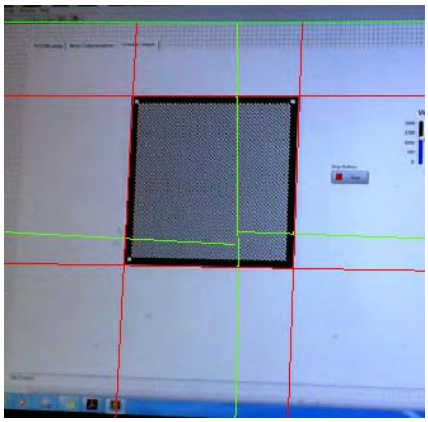

FIGURE 29. Practical Rx spatial sampling error due to bolder detection error and perspective distortion.

predicted if the focal length is fixed and attenuation due to the blur effect changes slowly.

To conclude this analytical subsection, several contributions are summarized as follows. The non-flat frequency response to the spatial OFDM system is observed in numerous experiments. More explicitly, the worst case of blur is frequency selective fading. This condition causes burst error within an OFDM symbol. Introducing an additional approach with FEC is proposed for dealing with the imperfect channel condition. Traditional FEC for OFDM in IEEE 802.11 [22] suggests CC or LDPC. However, the proposed combination of inner and outer FECs is naturally applicable and promising for the sequential transmission of OFDM symbols, especially spatial OFDM.

C. SPATIAL SAMPLING ERROR

1) SAMPLING SHIFT DUE TO CODE DETECTION

Let Δx and Δy be the shifted values in the space of the OFDM symbol caused by the error of code detection using the line (or corner) detection algorithm. Thus, the shifted sampling in space produces the phase shift in the frequency domain of the carrier $s_{p,q}$ and can be estimated as follows.

$$\widetilde{s_{p,q}} = s_{p,q} \exp\left(2\pi j(\frac{p\Delta_x}{L_x} + \frac{q\Delta_y}{L_y})\right) \tag{22}$$

where L_x and L_y are two sizes of a given 2D-FFT symbol.

When Rx makes the OFDM symbol with a shifted space $(\Delta x, \Delta y)$, the samples $S_{m,n}$ are formulated:

$$S'_{m,n} = \sum_{k=0}^{L_x-1}\sum_{l=0}^{L_y-1} s_{k,l} \exp\left(\frac{2\pi jk(m+\Delta_x)}{L_x} + \frac{2\pi jl(n+\Delta_y)}{L_y}\right) \tag{23}$$

The 2D-DFT calculates the estimated versions of 2D-carriers as follows

$$\begin{aligned}\widetilde{s_{p,q}} &= \frac{1}{\sqrt{L_xL_y}} \sum_{m=0}^{L_x-1}\sum_{n=0}^{L_y-1} S'_{m,n} \exp\left(-2\pi j(\frac{mp}{L_x} + \frac{nq}{L_y})\right) \\ &= \frac{1}{\sqrt{L_xL_y}} \sum_{m,n=0}^{L_x-1,L_y-1} S'_{m,n} \exp\left(-2\pi j(\frac{mp}{L_x} + \frac{nq}{L_y})\right)\end{aligned} \tag{24}$$

Substituting $S'_{m,n}$ from (29) to (24

$$\begin{aligned}\widetilde{s_{p,q}} &= \frac{1}{\sqrt{L_xL_y}} \sum_{m,n=0}^{L_x-1,L_y-1}\sum_{k,l=0}^{L_x-1,L_y-1} s_{k,l} \\ &\quad\times \exp\left(\frac{2\pi jk(m+\Delta_x)}{L_x} + \frac{2\pi jl(m+\Delta_y)}{L_y}\right) \\ &\quad\times \exp\left(-2\pi j(\frac{mp}{L_x} + \frac{nq}{L_y})\right) \\ &= \frac{1}{\sqrt{L_xL_y}} \sum_{m,n=0}^{L_x-1,L_y-1}\sum_{k,l=0}^{L_x-1,L_y-1} s_{k,l} \\ &\quad\times \exp\left(\frac{2\pi jk\Delta_x}{L_x} + \frac{2\pi jl\Delta_y}{L_y}\right) \\ &\quad\times \exp\left(2\pi j(\frac{m(k-p)}{L_x} + \frac{n(l-q)}{L_y})\right) \\ &= s_{p,q} \exp\left(2\pi j(\frac{p\Delta_x}{L_x} + \frac{q\Delta_y}{L_y})\right)\end{aligned} \tag{25}$$

Ascan be seen, the resulting carrier is the phase shifted version of the transmitted carrier. Also, the phase offset in the sampling is proportional to the distance shift of the Tx caused by the code detection. This resulting impact is reasonable.

2) SAMPLING ERROR BY PERSPECTIVE DISTORTION

Perspective distortion generates a captured Tx with unequal dimensions. Due to this, 2D-DFT should be implemented after the dimension sizes are corrected in the space-time domain to correct the distortion. Most of the related works, such as [15], dealt with the distortion this way and relied on the computer vision algorithm. However, the available distortion correction algorithm delays the processing time. A simple alternative approach to correct the dimension sizes is the downsampling process. A linear model of downsampling is introduced in this implementation (see Annex 2).

The remaining task is estimating the sampling error caused by perspective distortion and understanding the consequences. In fact, the linear model of downsampling applied for a non-linear perspective distortion should also generate phase shifts in addition to the phase shifts experienced by the code detection, given that the shift of the entire Tx in the space domain introduces the shift (i.e., offset) in the phase of the estimated carrier (see subsections 3.1). However, formulating the error caused by non-linear distortion is complex when transforming the space domain to the frequency domain.

The perspective distortion error in the space can be estimated as a convolution transformation by a calculable camera calibration matrix (usually denoted as the matrix K) and the offsets matrix of Tx (see [26]).

The correspondence between the worlds $(\widetilde{\mathbf{X}})$ and the pixel-points $(\widetilde{\mathbf{u}})$ in the image is described by a homogeneous matrix (3×4 size) and denoted as the camera projection matrix P.

$$\widetilde{\mathbf{u}} = \mathbf{P}\widetilde{\mathbf{X}} \tag{26}$$

$$\mathbf{P} = \mathbf{K}[R \quad t] = \begin{bmatrix} f & 0 & 0 \\ 0 & f & 0 \\ 0 & 0 & 1 \end{bmatrix} [R \quad t] \tag{27}$$

where K is the camera calibration matrix, and [R t] expresses the Euclidean transformation from the world dimensions {W} to the camera coordinate plan {C}.

$$\begin{bmatrix} {}^{w}X \\ {}^{w}Y \\ {}^{w}Z \\ 1 \end{bmatrix} \overset{[Rt]}{\mapsto} \begin{bmatrix} c_x \\ c_y \\ 1 \end{bmatrix} \overset{K}{\mapsto} \begin{bmatrix} u \\ v \\ 1 \end{bmatrix} \tag{28}$$

Fortunately, the convolution in the space-time domain is equivalent to the multiplication in the frequency domain (see Subsection 2.2). If the focal length is fixed and stable perspective distortion is assumed, the response in the frequency domain can be estimated for the channel adaptation.

The error caused by the downsampling process can be modeled as the attenuation of the magnitude and shift in the phase regarding the equivalent frequency response of the convolution function. Together, the detection error and downsampling process cause the attenuation.

To conclude this analytical subsection, several contributions are summarized as follows. Undeniably, the implementation of Rx is challenging for all communication systems. Suggestions for the specific Rx processes are disclosed with helpful approaches for correcting spatial sampling error. A 2D-OFDM Tx detection method (in conjunction with the rotation support) is proposed with a newly designed MIMO Tx, and the error of the spatial sampling system is comprehensively analyzed.

D. 2D CHANNEL CHARACTERISTICS

1) NONLINEARITY AND ATTENUATION

The nonlinearity of LEDs has been investigated in various VLC/LiFi studies. The non-linear I-V characteristic of a typical LED is subject of compensation. Similarly, the amplitude response of the screen-camera channel is also non-linear [15]. The conversion from perceived pixel intensity to bit energy was addressed in a previous work [3].

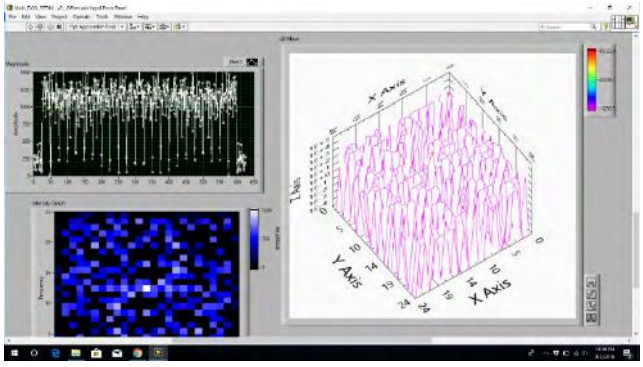

FIGURE 30. Real-time display of 2D-carriers attenuation measurement showing the time-variant characteristic.

A complex model for a non-linear channel is not recommended. As such, a nearly linear range of channel response can be found for the communication. This response measurement can be done as captured in Figure 30 and Figure 31.

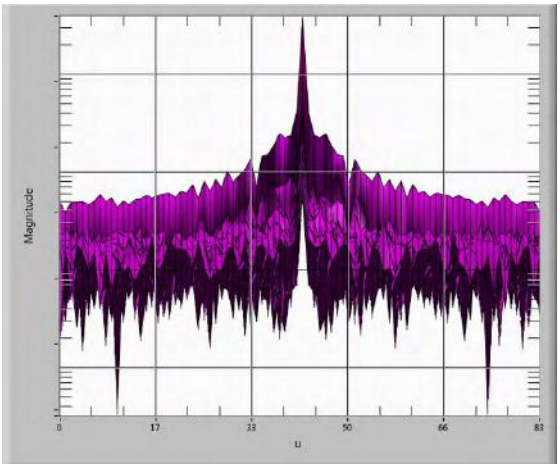

FIGURE 31. Experimental low-pass characteristic and frequency selective fading of Screen OFDM.

To deal with the limited linear range of a channel, the PAR in the OFDM waveform was not processed. Different PAR reduction techniques have been investigated previously. These techniques may rely on either introducing the redundancy or post-processing in the time domain waveform. Such coding schemes for a traditional OFDM in an RF system have been introduced in [5]. The clipping amplifier, one of the favored solutions for dealing with OFDM PAR without a complex coding scheme and redundancy scarification, was implemented with the proper clipping range, as analyzed in the next section.

2) CLIPPING NOISE

It has been previously found that the symmetric clipping process should be applied in the one-dimensional DCO-OFDM system [27]. In contrast, in the one-dimensional ACO-OFDM system, the bias clipping process at the top of the signal should be applied to the IFFT outputs to minimize the error caused by clipping. The conclusion applies to the 2D-OFDM system.

K was defined to be the attenuation factor of the clipping process and λ_{top}, λ_{bottom} were defined to be the top-clipping and bottom-clipping levels, respectively. Reference [28] introduced the equation

$$K = \frac{Cov[S_{m,n}, S_{clipped(m,n)}]}{\sigma^2_{S_{m,n}}} = Q(\lambda_{bottom}) - Q(\lambda_{top}) \tag{29}$$

where Cov[.] is the covariance operator and $\sigma^2_{S_{m,n}}$ is the variance of the signal $S_{m,n}$.

At the Rx, the double-slide clipped carriers were passed through the 2D-DFT:

$$s_{p,q} = \frac{1}{\sqrt{L_x L_y}} \sum_{m=0}^{L_x-1} \sum_{n=0}^{L_y-1} S'_{clipped(m,n)} \exp\left(-2\pi j(\frac{mp}{L_x} + \frac{nq}{L_y})\right) \tag{30}$$

According to [29], the effective electrical SNR per bit, $\Gamma_{b(elec)}$, can be expressed as

$$\Gamma_{b(elec)} = \frac{K^2 P_{b(elec)}/G_B}{\sigma_{clip}^2 + \frac{G_B \sigma_{AWGN}^2}{g_{h(opt)}^2 G_{DC}}} = \frac{K^2}{\frac{G_B \sigma_{clip}^2}{P_{b(elec)}} + \frac{G_B \gamma_{b(elec)}^{-1}}{g_{h(opt)}^2 G_{DC}}} \quad (31)$$

where Pb(elec) is the average electrical power of the bits; GB is the ratio of the utilized carriers (for ACO-OFDM, GB = 0.5, and for DCO-OFDM, GB is nearly 1); $g_{h(opt)}$ is the optical path gain coefficient; σ_{clip}^2 is the clipping noise variance. GDC is the attenuation of the electrical signal power over the non-linear I-V characteristic, and $\gamma_{b(elec)} = (E_{b(elec)}/N_o)$ is the SNR per bit.

Finally, the error caused by double-side clipping and white noise was estimated for M-QAM OFDM:

$$BER = \frac{4(\sqrt{M}-1)}{\sqrt{M}\log_2(M)} Q\left(\sqrt{\frac{3\log_2(M)}{M-1}\Gamma_{b(elec)}}\right) + \frac{4(\sqrt{M}-2)}{\sqrt{M}\log_2(M)} Q\left(3\sqrt{\frac{3\log_2(M)}{M-1}\Gamma_{b(elec)}}\right) \quad (32)$$

It can be seen from the final result that the selection of clipping levels is crucial and directly impacts the system performance. The clipping levels were selected experimentally. Examples of the clipping impact on the DCO-OFDM waveform are illustrated in Figures 32 and 33.

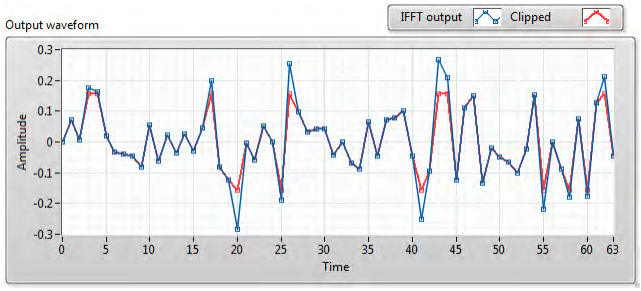

FIGURE 32. Example of a clipped waveform at the output of IFFT.

To conclude this analytical subsection, several contributions are summarized as follows. The distortion and noise due to the non-linear channel characteristic originate from the clipping process. The clipping thresholds are used by examining the channel condition via experiments. It has been stated in [5] that values within the range of 6 dB to 12 dB are the proper back-off clipping thresholds. 10 dB clipping was typically performed in the implementations.

ANNEX 2
Rx PROCESSING GUIDANCE

A. SPATIAL DOWNSAMPLING VS. PERSPECTIVE DISTORTION

The code must be detected (with acceptable performance) before the code area is extracted. Data decoding was performed after the extracted code was downsampled. In this screen-camera system, the code was designed to be

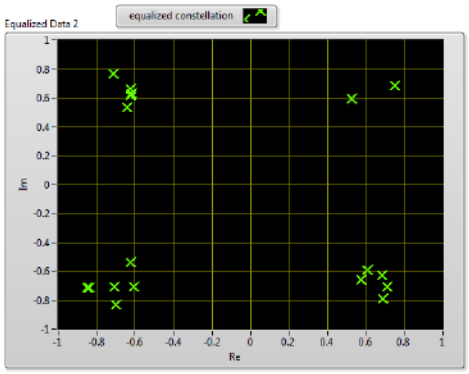

FIGURE 33. DCO-OFDM constellation diagram with both-sided clipping.

extractable when either the positions of the code corners or outer lines were determined.

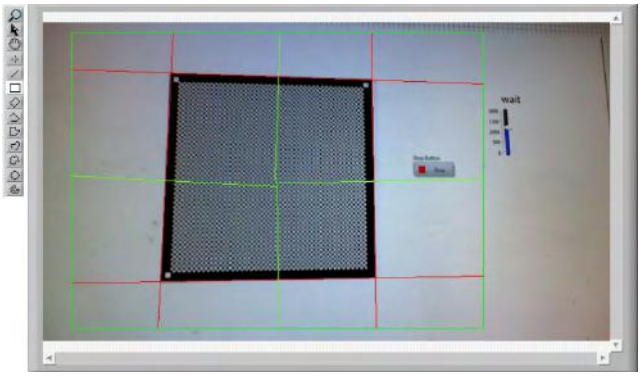

FIGURE 34. A screen interface at Rx with Tx detection using the proposed line detection.

The spatial extraction of the code follows this procedure:

Step 1: Detection of surrounding edges using image processing technique (see Figure 34). Edge detection is employed using a Hough transform. After that, spatial extraction of the entire code area defined by the surrounding edges is performed.

Step 2: Spatial downsampling for a linear fit of perspective-distorted code (see Figure 35). Notably, the presence of perspective distortion is canceled in this step.

The linear downsampling for non-linear perspective distortion causes the error in spatial sampling, as shown in Figure 35. The analysis of spatial sampling error, caused by either the detection error of the code or the imperfect correction of perspective distortion using 2D-pilots, was revealed in Annex 1 Section 3.

B. TEMPORAL DOWNSAMPLING VS. FRAME RATE VARIATION

A camera operating at the frame rate greater than the optical clock rate receives data by oversampling. However, as shown in the recently published study on the frame rate of cameras, the downsampling remains challenging for the time-variant frame rate Rx. Moreover, the challenge was unmitigated in related works, such as [15] and [16].

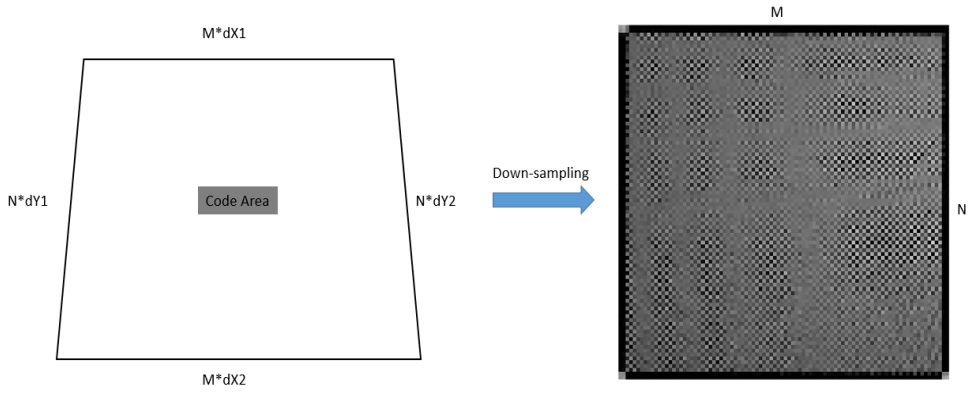

FIGURE 35. Down-sampling in the presence of perspective distortion.

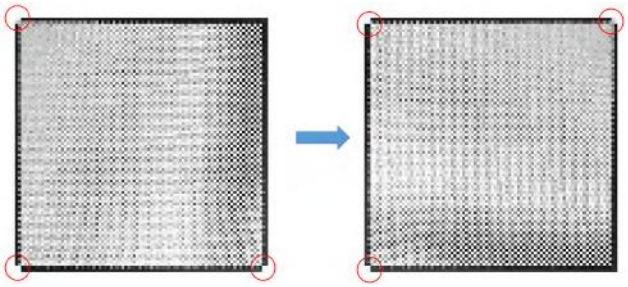

FIGURE 36. The experimental output of rotation correction.

Similar to the A-QL code system, an asynchronous bit(s) was added into the payload of each frame to support the downsampling process. The asynchronous bit(s) is a particular version of PHY sequence numbering so that Rx can distinguish adjacent frames and recover the superframe. The creation of asynchronous bits is a novel idea that solves the frame rate variation while keeping the redundancy at a minimum.

Practically, to support downsampling for an oversampled sequence, a single asynchronous bit is needed. This condition means that the frame rate of Rx needs to satisfy the requirement of oversampling (i.e., three times of the optical clock rate to avoid mixed sampling). However, in case Rx cannot satisfy the oversampling requirement, two or more bits can be used for frame numbering so that Rx can detect whether there is a missed frame for later link adaptation.

The inner FEC shall protect a packet of the asynchronous bit(s) and data bits as the payload of the frame.

C. ROTATION CORRECTION

The plurality of related screen-camera systems cannot support complete features like the QR code, and operation under rotation is one of the critical features that must be supported. Previously mentioned Screen OFDM systems have neglected this critical feature.

Given the code design, the rotation cells of Tx can support 360-degree rotation decoding in the same manner as that of the QR code. The rotation cells at four-corners of the Tx were binary-mapped so that they best minimized the consumed space. The experimental result is illustrated in Figure 36. Remarkably, the rotation correction using binary information transmitted via reference cells was more credible than the computer-vision-based identification of known corner patterns.

REFERENCES

[1] N. Serafimovski, V. Jungnickel, Y. M. Jang, and J. L. Qiang. (2017). *An Overview on High-Speed Optical Wireless/Light Communications*. Accessed: 2018. [Online]. Available: https://mentor.ieee.org/802.11/dcn/17/11-17-0962-02-00lc-an-overview-on-high-speed-optical-wireless-light-communications.pdf

[2] *IEEE Standard for Local and Metropolitan Area Networks—Part 15.7: Short-Range Wireless Optical Communication Using Visible Light*, IEEE Standard 802.15.7-2011, 2011.

[3] T. Nguyen, A. Islam, T. Hossan, and Y. M. Jang, "Current status and performance analysis of optical camera communication technologies for 5G networks," *IEEE Access*, vol. 5, pp. 4574–4594, 2017.

[4] T. Nguyen, A. Islam, T. Yamazato, and Y. M. Jang, "Technical issues on IEEE 802.15.7m image sensor communication standardization," *IEEE Commun. Mag.*, vol. 56, no. 2, pp. 213–218, Feb. 2018.

[5] L. Hanzo, M. Münster, B. Choi, and T. Keller, "*OFDM and MC-CDMA for Broadband Multi-User Communications, WLANs and Broadcasting*, Hoboken, NJ, USA: Wiley, 2003.

[6] F. A. Pinto-Benel, M. Blanco-Velasco, and F. Cruz-Roldán, "Throughput analysis of wavelet OFDM in broadband power line communications," *IEEE Access*, vol. 6, pp. 16727–16736, 2016.

[7] H. Hosseini, N. Fisal, and S. K. Syed-Yusof, "Wavelet packet-based multicarrier modulation for cognitive UWB systems," *Signal Process., Int. J.*, vol. 4, no. 2, pp. 75–84, 2010.

[8] A. Li, W. Shieh, and R. S. Tucker, "Wavelet packet transform-based OFDM for optical communications," *J. Lightw. Technol.*, vol. 28, no. 24, pp. 3519–3528, Dec. 15, 2010.

[9] W. Huang, C. Gong, and Z. Xu, "System and waveform design for wavelet packet division multiplexing-based visible light communication," *J. Lightw. Technol.*, vol. 33, no. 14, pp. 3041–3051, Jul. 15, 2015.

[10] J. Zhou *et al.*, "Low-PAPR layered/enhanced ACO-SCFDM for optical-wireless communications," *IEEE Photon. Technol. Lett.*, vol. 30, no. 2, pp. 165–168, Jan. 15, 2018.

[11] S. D. Dissanayake and J. Armstrong, "Comparison of ACO-OFDM, DCO-OFDM and ADO-OFDM in IM/DD systems," *J. Lightw. Technol.*, vol. 31, no. 7, pp. 1063–1072, 2013.

[12] M. R. H. Mondal, K. R. Panta, and J. Armstrong, "Performance of two dimensional asymmetrically clipped optical OFDM," in *Proc. IEEE Globalcom Workshop Opt. Wireless Commun.*, Dec. 2010, pp. 995–999.

[13] J. Volker *et al.* (2016). *HHI High-Rate PD Communication Proposal*. Accessed: 2018. [Online]. Available: https://mentor.ieee.org/802.15/dcn/16/15-16-0016-03-007a-proposal-for-tg7r1-high-rate-pd-communications.docx

[14] T. Dobroslav *et al.* (2016). *PureLiFi Low-Bandwidth PHY and MAC Proposal*. Accessed: 2018. [Online]. Available: https://mentor.ieee.org/802.15/dcn/16/15-16-0363-00-007a-text-input-lifi-low-bandwidth-phy-and-mac-d0.docx

[15] S. Hranilovic and F. R. Kschischang, "A pixelated MIMO wireless optical communication system," *IEEE J. Sel. Topics Quantum Electron.*, vol. 12, no. 4, pp. 859–874, Jul./Aug. 2006.
[16] S. D. Perli, N. Ahmed, and D. Katabi "PixNet: interference-free wireless links using LCD-camera pairs," in *Proc. MobiCom*, vol. 10, 2010, pp. 137–148.
[17] M. Rubaiyat H. Mondal, and J. Armstrong, "Analysis of the effect of vignetting on MIMO optical wireless systems using spatial OFDM," *J. Lightw. Technol.*, vol. 32, no. 5, pp. 922–929, Mar. 1, 2014.
[18] S. M. S. Sadough, M. M. Ichir, P. Duhamel, and E. Jaffrot, "Wavelet-based semiblind channel estimation for ultrawideband OFDM systems," *IEEE Trans. Veh. Technol.*, vol. 58, no. 3, pp. 1302–1314, Mar. 2009.
[19] M. N. Suma, S. V. Narasimhan, and B. Kanmani, "Orthogonal frequency division multiplexing peak-toaverage power ratio reduction by best tree selection using coded discrete cosine harmonic wavelet packet transform," *IET Commun.*, vol. 8, no. 11, pp. 1875–1882, 2014.
[20] *IEEE Standard for Broadband over Power Line Networks: Medium Access Control and Physical Layer Specifications*, IEEE Standard IEEE 1901-2010, 2010.
[21] X. Dong, W.-S. Lu, and A. C. K. Soong, "Linear Interpolation in Pilot Symbol Assisted Channel Estimation for OFDM," *IEEE Trans. Wireless Commun.*, vol. 6, no. 5, pp. 1910–1920, May 2007.
[22] *IEEE Standard for Information Technology—Telecommunications and Information Exchange Between Systems Local and Metropolitan Area Networks—Specific Requirements Part 11: Wireless LAN Medium Access Control (MAC) and Physical Layer (PHY) Specifications*, Standard 802.11-2012, 2012.
[23] I. B. Djordjevic, *Advanced Coding for Optical Communications*. Elsevier, ch. 6, 2013. [Online]. Available: https://www.oreilly.com/library/view/optical-fiber-telecommunications/9780123969606/xhtml/CHP006.html
[24] I. B. Djordjevic, "On advanced FEC and coded modulation for ultra-high-speed optical transmission," *IEEE Commun. Surveys Tuts.*, vol. 18, no. 3, pp. 1920–1951, 3rd Quart., 2016.
[25] D. A. Kerr. (2007). *Derivation of the 'Cosine Fourth' Law for Falloff of Illuminance Across a Camera Image*. Accessed: 2018. [Online]. Available: http://dougkerr.net/Pumpkin/articles/Cosine_Fourth_Falloff.pdf
[26] T. Opsahl. *Lecture 1.4 The Perspective Camera Model*. Accessed: 2018. http://www.uio.no/studier/emner/matnat/its/UNIK4690/v16/forelesninger/lecture_1_4-the-perspective-camera-model.pdf
[27] S. Dimitrov, S. Sinanovic, and H. Haas, "A comparison of OFDM-based modulation schemes for OWC with clipping distortion," in *Proc. IEEE GLOBECOM Workshops (GC Wkshps)*, Houston, TX, USA, 2011, pp. 787–791.
[28] S. Randel, F. Breyer, S. C. J. Lee, and J. W. Walewski, "Advanced modulation schemes for short-range optical communications," *IEEE J. Sel. Topics Quantum Electron.*, vol. 16, no. 5, pp. 1280–1289, Sep./Oct. 2010.
[29] S. Dimitrov, S. Sinanovic, and H. Haas, "Clipping noise in OFDM-based Optical Wireless Communication Systems," *IEEE Trans. Commun.*, vol. 60, no. 4, pp. 1072–1081, Apr. 2012.

TRANG NGUYEN received the Engineering degree in biomedical engineering from the Hanoi University of Science and Technology, Vietnam, in 2013, and the M.Sc. and Ph.D. degrees in electrical and electronics engineering from Kookmin University (KMU), South Korea, in 2015 and 2018, respectively.

His research interests include optical wireless communications (OWC), optical networks, wireless systems, optical camera communications (OCC), and augmented-reality services via light. He has designed and implemented a variant of OWC/OCC systems. Mainly from 2013 to 2018, he has a dominant contribution to six international patents/applications +37 other Korea patents/applications while being an implementation lead of over 10 registered software applications; some of these works have been published as several highly cited journal papers. Also, he is leading abundant projects involving in the advanced development of OWC/OCC technologies.

He is currently a Researcher with the LED Convergence Research Center, KMU, and continues as a Voting Member of the IEEE 802.15. He is the Creator of OpticalPress.com, a website for discussing OWC/OCC technologies and sharing the open source.

MINH DUC THIEU received the bachelor's degree in control and automation engineering technology from the Hanoi University of Science and Technology, Vietnam, in 2015. He is currently pursuing the M.Sc. degree in electrical and electronics engineering with Kookmin University, South Korea.

His research interests include optical wireless communications, wireless communication systems, optical camera communications, and optical V2X communication.

YEONG MIN JANG received the B.E. and M.E. degrees in electronics engineering from Kyungpook National University, South Korea, in 1985 and 1987, respectively, and the Ph.D. degree in computer science from the University of Massachusetts, USA, in 1999.

He was with the Electronics and Telecommunications Research Institute, from 1987 to 2000. Since 2002, he has been with the School of Electrical Engineering, Kookmin University, Seoul, South Korea, where he has been the Director of the Ubiquitous IT Convergence Center, since 2005, and the Director of the LED Convergence Research Center, since 2010. His research interests include 5G mobile communications, multiscreen convergence, public safety, optical wireless communications, optical camera communication, and the Internet of Things.

Dr. Jang is currently a Life Member of the Korean Institute of Communications and Information Sciences (KICS). He received the Young Science Award from the Korean Government, from 2003 to 2006. He has organized several conferences and workshops, such as the International Conference on Ubiquitous and Future Networks, from 2009 to 2016, the International Conference on ICT Convergence, from 2010 to 2016, the International Conference on Information Networking, in 2015, and the International Workshop on Optical Wireless LED Communication Networks, from 2013 to 2016. He had served as the Founding Chair for the KICS Technical Committee on Communication Networks, in 2007 and 2008. He had served as the Executive Director of KICS from 2006 to 2014 and the Vice President of KICS from 2014 to 2016. He had served as the Chairman of the IEEE 802.15 Optical Camera Communications Study Group in 2014. He is currently serving as the Chairman of the IEEE 802.15.7m Optical Wireless Communications Task Group. He is also the Chairman of the IEEE 802.15 Vehicular Assistive Technology Interest Group. He serves as the Co-Editor-in-Chief for *ICT Express* (Elsevier). He has been the Steering Chair of the Multi-Screen Service Forum since 2011 and the Society Safety System Forum since 2015.